Effects of Confinement and External Fields on Structure and Transport in Colloidal Dispersions in Reduced Dimensionality

D. Wilms[1,2], S. Deutschländer[3], U. Siems[3], K. Franzrahe[3], P. Henseler[3], P. Keim[3], N. Schwierz[3], P.Virnau[1], K. Binder[1], G. Maret[3], P. Nielaba[3]

[1]Institut für Physik, Johannes Gutenberg-Universität Mainz, Staudinger Weg 7, D-55099 Mainz, Germany

[2]Graduate School Materials Science in Mainz, Staudinger Weg 9, D-55128 Mainz, Germany

[3]Physics Department, University of Konstanz, 78457 Konstanz, Germany

E-mail: wilmsdo@uni-mainz.de

Abstract. In the present work, we focus on low-dimensional colloidal model systems, via simulation studies and also some complementing experiments, in order to elucidate the interplay between phase behavior, geometric structures, and transport properties. In particular, we try to investigate the (nonlinear !) response of these very soft colloidal systems to various perturbations: uniform and uniaxial pressure, laser fields, shear due to moving boundaries, and randomly quenched disorder.

We study ordering phenomena on surfaces or in monolayers by Monte Carlo computer simulations of binary hard-disk mixtures, the influence of a substrate being modeled by an external potential. Weak external fields allow a controlled tuning of the miscibility of the mixture. We discuss the involved, underlying ordering mechanism, i.e. Laser Induced De-mixing. For the field-free case we discuss the thermodynamic stability of space-filling lattice structures.

The structural behavior of hard spheres interacting with repulsive screened Coulomb or dipolar interaction in 2D and 3D narrow constrictions is investigated using Brownian dynamics simulations. The system of particles adapts to the confining potential and the interaction energies by a self-consistent arrangement of the particles. It results in the formation of layers or planes throughout a microchannel. The arrangement of the particles is perturbed by diffusion and an external driving force leading to a density gradient along the channel. The particles accommodate to the density gradient by reducing the number of layers or planes if it is energetically favorable. The influence of a self-organized order within the system is reflected in the velocity of the particles and their diffusive behavior.

Additionally, in an experimental system of dipolar colloidal particles confined by gravity on a solid substrate we investigate the effect of pinning on the dynamics of a two-dimensional colloidal liquid.

1. Introduction

Soft matter with its structural and elastic properties offers an attractive route to the design of new materials. The importance of structured surfaces or monolayers lies in their promising, versatile technical applicability. Examples are antireflection surfaces, optical storage media or the usage in template-directed colloidal crystallization, the resulting three-dimensional colloidal crystals being, e.g., of interest due to their tailored photonic band gaps. The physics of surfaces and adsorbed monolayers has attracted a lot of interest in this context. In theoretical studies two dimensional systems are often used as a model, the interactions with substrates being conveniently modeled by external fields. The experimental counterpart, two-dimensional systems of colloidal suspensions, has been studied extensively in the last decades. They offer direct access to real space data via laser scanning microscopy, an excellent control over the colloidal interactions and easy tunability of the substrate potential in its shape and strength, as it is modeled, e.g., by interference patterns of laser beams. A close interplay between experiments, analytic theory, and computer simulations helped to shed light on such fundamental questions of statistical physics as the nature of melting in two dimensions with and without the influence of external fields. The interaction of monodisperse, two dimensional systems with one-dimensional, periodic light fields lead to the discovery of complex phase behavior as for example laser induced freezing and laser induced melting. Elastic properties of two-dimensional colloidal crystals have been analysed by us recently [1, 2], as well as the effect of external fields on structures and phase transitions [3, 4, 5, 6, 7].

Particularly with respect to the interest in complex, two dimensional structures for the design of new materials and the rich phase behavior resulting from the interaction of monodisperse systems with simple external light fields, questions arise, as to what complex, periodic structures binary mixtures might assemble in, and what influence an interaction with simple external light fields has on the phase behavior of such mixtures. In [3] we focussed in particular on the differences in the induced ordering and ordering mechanisms that result from the various possible interaction scenarios with the external potential in a mixture. Binary hard-disk mixtures are chosen as a model system for the clarification of these questions. Hard-disks are neither selective in the choice of the type of next-neighbor particles nor in the number of next-neighbor particles. Therefore the model system is ideal to show what ordering can result solely from geometric constraints due to the diameter ratio σ_B/σ_A of the components of the mixture and due to the concentration of the mixture. These characteristics make them also a good model for the ground state of atomic systems with short range interactions.

In the present work, we focus on such low-dimensional colloidal model systems, via simulation studies and also some complementing experiments, in order to elucidate the interplay between phase behavior, geometric structures, and transport properties. In particular, we try to investigate the (nonlinear !) response of these very soft colloidal systems to various perturbations: uniform and uniaxial pressure, laser fields, shear due

to moving boundaries, and randomly quenched disorder.

The manuscript is organized as follows: In the next section we present the results of Monte Carlo studies of the structures and phase diagrams of binary hard disk mixtures at high pressures or in external fields. In section 3 we show Monte Carlo simulation results of the effect of one-dimensional confining corrugated walls on phase transitions of two-dimensional colloidal crystals and on their behavior under shear. Section 4 presents our results of Brownian Dynamics simulation studies of transport of colloidal systems in two- and tree-dimensional channels, and in section 5 experimental results of the pinning effect on the dynamics of a two-dimensional colloidal liquid are presented.

2. Binary two-dimensional Model Colloids in External Fields

We modelled [3] the analyzed, binary, two-dimensional mixtures by $N = N_A + N_B$ hard-disks. The diameter of the larger component of the mixture is set to σ_A=1 in all simulations. All lengths are measured in units of σ_A. The packing fraction of the mixture is defined as $\eta = \rho^* \pi (N_A \sigma_A^2 + N_B \sigma_B^2)/4N$, where $\rho^* = \rho \sigma_A^2$ is the dimensionless number density. The concentration of large particles in the mixture is given by $x_A = N_A/N$. The mixtures under study are additive mixtures. Information on the equilibrium phase behavior of these mixtures is obtained via Monte Carlo computer simulations. Periodic boundary conditions are employed in all simulations. Besides the standard Metropolis algorithm a cluster move by Lue [8] is employed.

2.1. High Pressure Phases without External Fields

Simulations [3] in the NpT ensemble were used for testing the thermodynamic stability of given lattice structures. Here the simulation volume can fluctuate although shearing the simulation box was not attempted. In these studies suggested space-filling lattice structures for various binary mixtures [9] were set up with $N \approx 1000$. Simulations were run starting from a high, hydrostatic external pressure $p^* = p\sigma_A^2/k_BT$ and lowering it in successive runs. The resulting change in packing fraction η with pressure p^* was monitored. After equilibrating the system for 10^6 Monte Carlo steps (MCS), data were taken for another 2×10^6 MCS. $S_1(AB)$ square lattice structures were set up and simulated for σ_B=0.392, 0.396, 0.400, and 0.414. Figure 1(a) shows the packing fraction η as a function of decreasing pressure p^*, as it is obtained from simulations. The discontinuous decrease in η signifies the transition from the ordered phase to the fluid phase. The square lattice structure is stable for $p^* \geq 32$ for all simulated mixtures. $H_2(AB)$ lattice structures were set up and simulated for σ_B=0.627, 0.638, 0.640, and 0.646. The packing fraction as a function of decreasing pressure p^* is plotted in Fig.1(b). This lattice structure stays stable in systems with $p^* \geq 20$ for the analyzed mixtures. In Fig.1(b) the stability of the $H_2(AB)$ structure increases as the diameter of the smaller particles σ_B gets larger. This can be understood, if one recalls that as $\sigma_B \rightarrow 1$ the $H_2(AB)$ structure transforms directly into the monodisperse triangular lattice structure.

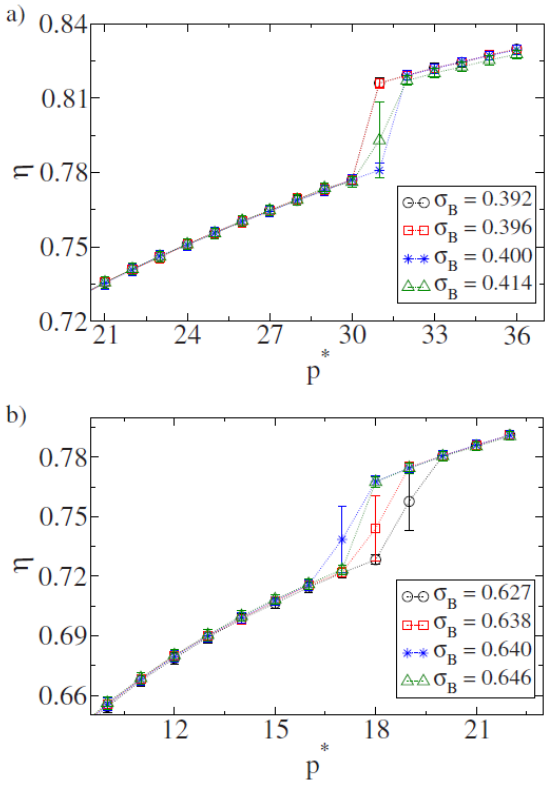

Figure 1. The packing fraction η as a function of decreasing pressure p^* in an equimolar binary mixture. Two different lattice structures are tested for their stability: (a) the $S_1(AB)$ square lattice for various mixtures with $\sigma_B/\sigma_A \in [0.392,0.414]$. (b) The $H_2(AB)$ lattice for mixtures with $\sigma_B/\sigma_A \in [0.627,0.646]$. After Franzrahe et al. [3].

In comparison a higher external pressure is needed in order to stabilize a $S_1(AB)$ square lattice structure in the equimolar mixture.

An overview of the simulated binary mixtures is given in Fig.2. For illustration sketches of the studied lattice structures are shown. Also given are the packing fraction η and the pressure p^*, above which all of the simulated mixtures were found to be stable for the given lattice structures. Figure 2 shows that the more a given lattice structure deviates from the triangular, monodisperse lattice the higher the hydrostatic pressure needed to stabilize it. The simulations show that the complex, space-filling lattice structures for binary hard-disk mixtures are high pressure phases. This makes it difficult to observe such structures in experimental set ups, as by increasing the pressure within the surface the probability that the monolayer will escape into the third dimension by buckling will also increase. These findings show clearly the importance of the search for alternative ways to stabilize or induce the formation of ordered structures in two dimensional, binary mixtures. One promising approach is the use of external fields.

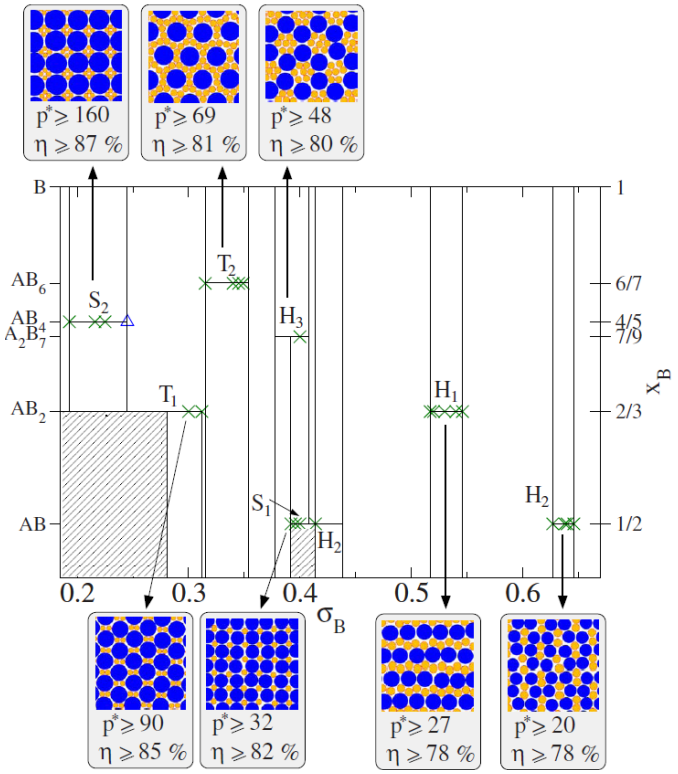

Figure 2. Overview of analyzed lattice structures for binary hard-disk mixtures. Structures for which a pressure regime, in which the structures stay stable, could be identified are marked by crosses (green). For the mixture marked by a triangle (blue) the lattice structure was not stable within the simulated pressure regime of $p^* \leq 200$. Also given are the packing fraction η and the pressure p^* above which all of the simulated mixtures for the given lattice structure were found to be stable. After Franzrahe et al. [3].

2.2. Effects of External Fields

Monodisperse 2D colloidal systems in interaction with a substrate potential have been studied extensively in experiments [10, 11], computer simulations [12, 6, 13, 5] and theory [14, 15, 16] over the last decades. Reentrant phase transition scenarios like *Laser Induced Freezing* (LIF) and *Laser Induced Melting* (LIM) have been observed. In a recent study [3] we addressed the question of how the addition of another length scale into such a system influences the intricate competition between adsorbate-adsorbate and adsorbate-substrate interaction by studying a binary 50% mixture under the influence of a 1D spatially periodic substrate potential. The colloids are modelled by hard disks with a diameter ratio $\sigma_B/\sigma_A = 0.414$. Following the approaches in the monodisperse studies, we use the following external potential: $V(\vec{r}) = V_0 \sin(\vec{K} \cdot \vec{r})$ with $\vec{K} = (4\pi/a, 0)$ and a the lattice parameter of the $S_1(AB)$ lattice. Thus the wavelength $\lambda = 2\pi/|\vec{K}|$ of the external potential is commensurate to the periodicity of the $S_1(AB)$ lattice.

The influence of a modulated external field was analyzed [3] by Monte Carlo simulations in the NVT ensemble. In these simulations additional nonlocal moves

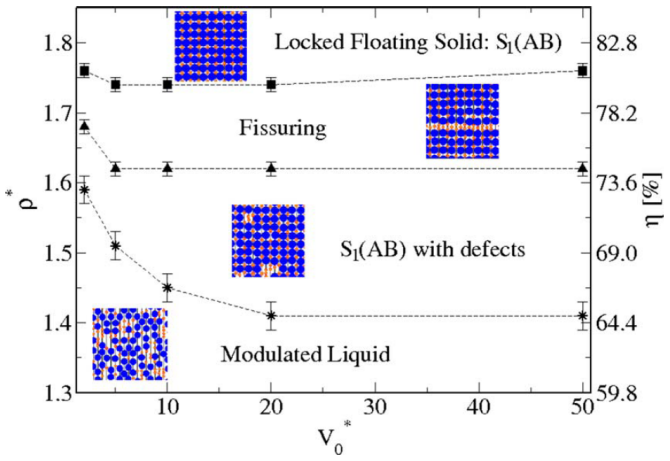

Figure 3. The phase diagram for an equimolar binary mixture with diameter ratio $\sigma_B/\sigma_A = 0.414$ exposed to an external periodic potential, commensurate to the $S_1(AB)$ square lattice for the case that both components of the mixture interact with the external potential [3]. The fissuring regime and the $S_1(AB)$ lattice with defects are stabilized down to far lower packing fractions η as compared to case (I) (see Franzrahe et al. [4]). Lines are a guide to the eye. After Franzrahe et al. [3].

are attempted with particle displacements, which are integer multiples of the potential wavelength. The simulation box is set up to be slightly rectangular with $L_x/L_y \approx 1.178$ and $N = 1848$ for these simulations. This choice allows not only a box-spanning square lattice to form, but also a box-spanning monodisperse triangular lattice of the larger component can develop. After equilibrating the system for 10^7 Monte Carlo steps (MCS) the simulations were run for another 10^7 MCS and data were taken.

For the interaction of the mixture with the external field three cases can be distinguished: (I) only the smaller component interacts with the external field [4], (II) both components interact with the external field, (III) only the larger component interacts with the external field.

For low amplitudes $V_0^* = V_0/k_BT$ we found a novel phenomenon: in contrast to the monodisperse LIF scenario a Laser Induced De-mixing [4] sets in for all three cases. Laser induced demixing results in the coexistence of a small component enriched fluid with a droplet of a mono- disperse crystalline structure formed by the larger component. The ordering mechanisms at work and the resulting monodisperse lattice structures differ for the three cases [3]. The ordering mechanisms stem from the attempt of the system to minimise its energy via an alignment of the components interacting with the external potential with the potential minima and the constraint of a fixed overall number density. While the coupling of only the smaller component to the external potential (case (I)) results in the coexistence of a monodisperse triangular lattice, the cases (II) and (III), where the larger component interacts directly with the external potential, show a condensation of a monodisperse rhombic lattice.

Further interesting phenomena arise from the fact, that the laser induced melting transition, as it occurs in monodisperse systems, is geometrically blocked in the binary

mixture studied in [3]. This leads to an enhanced stabilisation of the locked floating solid, a $S_1(AB)$ crystal. The phase diagram for the case that both components interact with the external field (case (II)) is shown in Figure 3 [3].

Here an increase in the amplitude of the external potential at constant density leads to a competition between rhombic, monodisperse domains of the large component and square lattice domains. As the rhombic domains are directly stabilised by the external potential, these structures hamper the growth of the square lattice domain. The resulting lattice structure is a $S_1(AB)$ square lattice with frozen in disorder. A comparison of the phase diagrams for case(I)[4] and (II) shows that both phase boundaries, the one from the fissuring regime to the $S_1(A)$ lattice with frozen in disorder and the one to the Modulated Liquid, are shifted to considerably lower packing fractions for the case that both components of the mixture couple to the external potential[3]. This is due to the direct stabilisation by the external field of the occurring ordered phases.

3. Two-Dimensional Colloidal Crystals Confined by One-Dimensional Corrugated "Walls": Phase Transitions and Behaviour under Shear

In this section we discuss simulation studies of a system of spherical colloids (which we model by point particles) interacting with each other via a short-ranged isotropic repulsive potential in a two-dimensional geometry and which are confined by corrugated repulsive walls (Fig. 4). Following our previous work [17, 18, 19, 20, 21], we define these walls in terms of two rows of particles fixed at the positions of a (perfectly ideal) rigid triangular lattice, which has a spacing commensurate with the lattice structure of the mobile particles (at the chosen density), see Fig. 4.

For our Monte Carlo simulations, we choose a generic model which is computationally efficient: a potential $V(r) \propto r^{-12}$, but cut off at a finite range r_c (and shifted and smoothed, to avoid problems resulting from discontinuous forces). Specifically, we use

$$V(r) = \left[\epsilon \left(\frac{\sigma}{r}\right)^{12} - \epsilon \left(\frac{\sigma}{r_c}\right)^{12}\right] \cdot \left[\frac{(r-r_c)^4}{h^4 + (r-r_c)^4}\right] \tag{1}$$

with parameters $r_c = 2.5\sigma$, $h = 0.01\sigma$, and the particle diameter $\sigma = 1$ defining the length scale in our model. Similarly, $\epsilon = 1$ defines the energy scale. At a density $\rho = N/V = 1.05$ the melting transition then occurs at a temperature $T = T_m = 1.35$ [22] (note $k_B = 1$). We are mostly interested in temperatures $T = 1.0$ or lower here, i.e. deep in the crystalline phase.

Already in our previous work it was shown that uniaxial compression of the system by reducing the available (two-dimensional) "volume" via a reduction of the distance D between the confining walls can introduce structural phase transitions in the system [19, 20, 21]. Increasing the misfit Δ (defined via $D(\Delta) = (n_y - \Delta)a\sqrt{3}/2$, $D(0) = D_0$, a being the lattice constant of the undistorted triangular lattice at the chosen density $\rho = N/(D_0 L_x) = 1.05$) one finds that the stress anisotropy $\sigma = \sigma_{yy} - \sigma_{xx}$ increases until

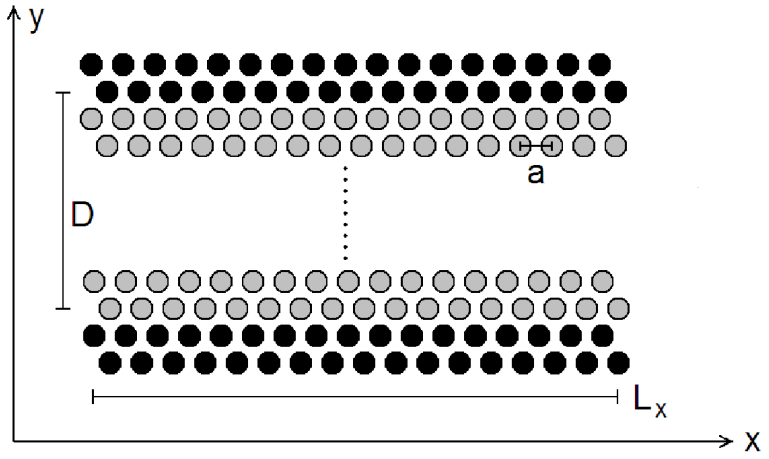

Figure 4. Sketch of the system geometry, showing the fixed wall particles (black spheres) and the mobile particles (grey spheres). The orientation of the coordinate axes is indicated, as well as the lattice spacing a of the triangular lattice and the linear dimensions L_x and D of the system. When $D = n_y a\sqrt{3}/2$ there is no misfit, n_y rows of mobile particles (containing n_x particles each, $L_x = n_x a$) occur at the approximately ideal distances relative to each other, while the choice $D = (n_y - \Delta)a\sqrt{3}/2$ (with the misfit Δ) implies uniaxial compression of the lattice. Typically we work with $n_y = 30$ rows and $n_x = 108$ (i.e., $N = 3240$ mobile particles). Note that shear can be introduced in the system by moving the lower wall with velocity v_{shear} in the $+x$-direction and the upper wall with the same velocity in the $-x$-direction.

at some value a jump discontinuity occurs, where σ suddenly decreases, accompanied by a transition where the number of rows changes ($n_y \to (n_y - 1)$) while the total particle number N in the system stays fixed.

This reduction in the number of layers means, that the n_x particles of the row that is removed are distributed in the remaining rows, leading to a smaller lattice spacing also in x-direction. However, this smaller lattice spacing is incommensurate with the original lattice spacing a in the rows of fixed particles representing the walls: this lack of commensurability leads to the formation of a "soliton staircase" along the boundaries, and a nonuniform strain distribution throughout the system [19, 20, 21].

However, when one follows this transition in the opposite direction ($(n_y - 1) \to n_y$), one encounters a huge hysteresis (Fig. 5). Such a nonequilibrium behaviour is not uncommon for discontinuous (first order) phase transitions, of course. Note that the situation gets worse when one compresses the system further, to observe the transition $(n_y - 1) \to (n_y - 2)$ (Fig. 5). Several "candidate structures" for the phase with $n_y - 2$ rows were found, but a priori it is unclear which is stable and which are only metastable.

To clarify the relative stability of such structures which are imperfectly crystallized and to locate the positions of the transitions in thermal equilibrium, a first principle method is to obtain the free energy difference between the various structures. There are several methods how this can be done. One approach that we have applied is to use the method of Schmid and Schilling [22] which separately estimates the absolute free energy

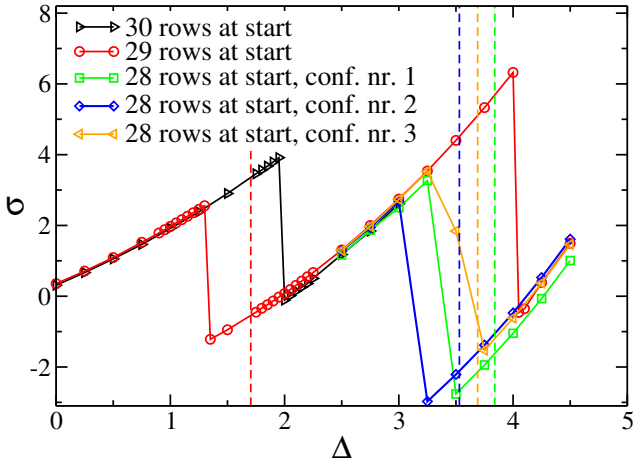

Figure 5. Stress anisotropy $\sigma = \sigma_{yy} - \sigma_{xx}$ plotted vs. misfit Δ, for a system of $N = 3240$ mobile particles, and using different starting configurations, containing either $n_y = 30$ or $n_y = 29$ or $n_y = 28$ rows. The vertical broken straight lines denote the positions of the equilibrium transitions, located by free energy methods. Note that the phase switch simulations [23] showed that from the 3 candidate structures nrs. 1-3 with 28 rows the structures nr. 1 and 3 are only metastable, while nr. 2 is the stable structure. All data are for $T = 1.0$.

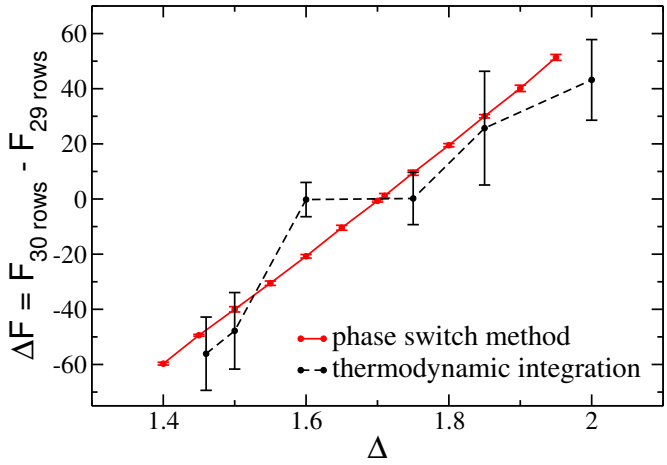

Figure 6. Free energy differences between the structures with $(n_y - 1) = 29$ and $n_y = 30$ rows shown as functions of the misfit Δ. The points with the large error bars are from the Schmid-Schilling thermodynamic integration method, the points falling on the straight line are from phase switch Monte Carlo simulations. After Wilms et al. [23].

of each structure in question. However, the obvious disadvantage of this method is that, for the transition from $n_y = 30$ to $n_y = 29$, for a misfit in the range $1.4 \leq \Delta \leq 2.0$, the total free energies F_I, F_{II} of both phases vary from about 22000 to about 24000, but their difference ΔF varies only from about -60 to $+60$ in that range. Thus reaching the necessary accuracy requires an enormous effort. We have found it much more efficient (see [23] for a more detailed explanation of technical aspects of this work) to employ the "phase switch Monte Carlo method" [24, 25]. In this method, one directly carries

out moves from states belonging to one phase to states belonging to the other phase, sampling the relative weights of both phases in the course of the simulation. Fig. 6 shows, as an example, a plot of ΔF vs. Δ for the $n_y \to (n_y - 1)$ transition [23].

Having clarified which structures are stable and which are only metastable, it is of interest to explore the response of the system when the walls are sheared against each other (Fig. 7). One sees that the shear deformation "melts" the crystal near the walls, where the velocity is nonzero, so the particles flow with the wall. Note that unlike Figs. 5, 6 these data are not obtained from Monte Carlo methods, of course, but rather using Molecular Dynamics methods (applying a Langevin thermostat to avoid that the system steadily heats up: we do find at large velocities a nontrivial temperature profile $T(y)$ across the film, however [26]).

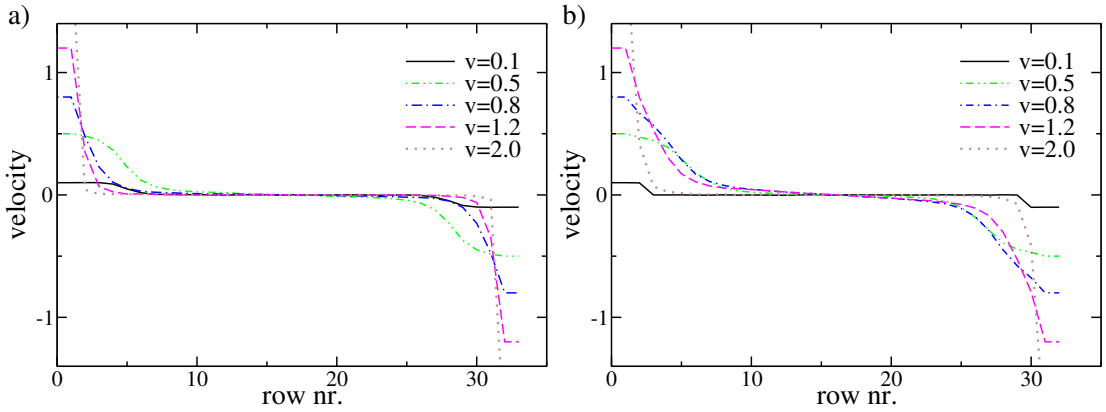

Figure 7. Velocity profile $v(y)$ at temperature $T = 0.3$ and $n_y = 30$, $\Delta = 0$, i.e. a commensurate system with no misfit (a) and a system with $n_y = 29$ rows at misfit $\Delta = 2.2$ (b). Various choices of the wall velocity v_{shear} are included, as indicated.

One should not attribute the shear melting of the crystal near the walls to the increase in local temperature (which is extracted from the velocity distribution of the particles), however: as Fig. 7 demonstrates, the range over which the velocity is distinctly nonzero in the system is largest for a wall velocity of $v = 0.5$, for which the temperature enhancement near the walls is still small. I.e., about 5 rows at each wall are taking in this case fluid like configurations, as an examination of snapshot pictures reveals. It should also be noted that in the interior of the system the triangular crystal structure does not at all stay intact: rather one finds large crystalline domains rotated by more or less large angles relative to the undeformed case. These domains are separated by grain boundaries. This structure is not completely static: in fact, for row numbers $n = 10$ or $n = 20$, which belong to this crystalline domain structure, one finds small but distinctly nonzero velocities (for wall velocity $v = 0.5$, for instance): thus, the system exhibits plastic flow.

When the wall velocity increases beyond about $v = 1.5$, however, the extent of flow that is caused in the system is much reduced: the wall particles already move too fast to be able to create a coherent motion in the boundary region of the crystalline strip.

In fact, for $v \to \infty$ the situation corresponds to an effectively flat wall potential, which does not lead to any flow of the mobile particles. Also the local temperature increases only in the rows immediately adjacent to the walls (due to enhanced friction), while in the interior of the system $T(y)$ with increasing v reaches a maximum and then decreases again.

Thus, shearing confined two-dimensional (and hence very soft) crystals causes a very rich and diverse behaviour (for a more detailed account of this work we refer to [26]).

4. Transport in Colloidal Model Systems

While the equilibrium properties of colloidal systems in bulk are extensively studied and understood by now, important questions concerning colloids in confined geometries or in non-equilibrium are still open [27]. Such systems can serve as model systems for complex processes such as the dynamic behavior of lattice defects, the transport of interacting particles through narrow constrictions, which is important in biological systems like ion channels [28], or non-equilibrium transport and mixing phenomena on the micrometer scale in the context of microfluidics and "lab-on-a-chip" devices [29]. The advantage of using colloidal systems as model systems is that they are experimentally easily accessible and can help to understand the underlying physics governing complex processes.
The formation of lanes along the direction of motion is a prominent feature and occurs in various system with interacting entities like pedestrians in a pedestrian zone [30] or ants following a trail to food places. For colloidal particles this formation of layers has been studied both in two-dimensional (2D) [31, 32, 33] and in three-dimensional (3D) systems [34, 35, 36]. So far there are no experimental studies for such systems. However, first hints for a lane formation transition occur in oppositely charged colloids driven in opposite directions by an electric field [37] or in binary complex plasmas under microgravity conditions [38]. The transport behavior of superparamagnetic colloids confined in 2D microchannels has been investigated both experimentally and by Brownian Dynamics simulations [39, 40]. Such driven, diffusive systems serve as model systems for the theoretical studies of non-equilibrium behavior [41]. Due to a confinement, a classical 2D system forms a layered structure in equilibrium [42, 17] and the change in the number of layers due to the geometry of the confinement has been predicted using Langevin Dynamic simulations [43]. The layers in the macroscopic transport can be seen as analogous to quantum channels since in both transport occurs due to the interaction of the particles with the confining potential.

In [44] we investigated the structural behavior of particles interacting via a hard-core Yukawa (YHC) potential in 2D and 3D microchannels by Brownian Dynamics simulations. The Brownian Dynamics simulations are based on the overdamped Langevin equation, neglecting hydrodynamic interactions as well as short time momentum relaxation of the particles. The colloidal trajectories are approximated by

the stochastic position Langevin equation with the friction constant ξ

$$\xi \frac{d\mathbf{r}_i(t)}{dt} = -\nabla_{\mathbf{r}_i} \sum_{i \neq j} \mathcal{V}_{ij}(r_{ij}) + \mathbf{F}_i^{(ext)} + \tilde{\mathbf{F}}_i(t). \tag{2}$$

The right-hand side includes the particle interaction as a sum over all forces acting on each particle, the constant driving force $\mathbf{F}_i^{(ext)}$ and the random forces $\tilde{\mathbf{F}}_i$ describing the random collisions of the solvent molecules with the i-th colloidal particle. The latter is in the simulation given by a random number with zero mean $\left\langle \tilde{\mathbf{F}}_i(t) \right\rangle = 0$ and variance $\left\langle \tilde{\mathbf{F}}_{i\alpha}(t) \tilde{\mathbf{F}}_{j\beta}(0) \right\rangle = k_B T \delta(t) \delta_{ij} \delta_{\alpha\beta}$ where k_B denotes the Boltzmann constant, T the temperature and the subscripts α and β the Cartesian components. Eq. (2) is integrated forward in time using a finite time step Δt and the technique by Ermak [45]. A density dependent cut-off is used for the interaction potential which has a value of $R_{\text{cut}} = 6.5 * R$ where $R = (2\rho/\sqrt{3})^{-1/2}$ in the 2D systems and $R = \rho^{-1/3}$ in the 3D systems. The 2D channels have a length of $L_x = 800\sigma$ and a width of $L_y = 10\sigma$ containing 3200 particles corresponding to a density of $\rho = 0.4\sigma^{-2}$. The 3D channels have a quadratic square section of $L_y = L_z = 5\sigma$ and a length of $L_x = 1000\sigma$ containing about 10000 particles with a fixed particle density of $\rho = 0.4\sigma^{-3}$. The particles are confined within the channels by ideal hard walls. The equilibrium configuration in a closed channel is calculated starting from a random configuration and applying hard wall boundary conditions in all directions. The systems are typically equilibrated over 2×10^5 time steps. The time step $\Delta t = 7.5 \times 10^{-5} t_B$ is used where $t_B = \xi \sigma^2 / k_B T$ is the time a particle needs in equilibrium to diffuse its own diameter σ. The friction constant ξ is chosen to be $\xi = 3\pi\eta\sigma = 4,288 * 10^{-8}$ Ns/m where $\eta = 0.001$ Pa*s is the shear viscosity of water. The simulations are done at a constant temperature $T = 295$ K. To study the influence of an external force, a constant driving force of $F_{\text{ext}} = 2.603 * 10^{-15}$ N is applied in longitudinal direction. The channel end is then realized by an open boundary condition. To keep the number density in the channel fixed a new particle is inserted within the first 10% of the channel at a random position avoiding overlaps every time a particle leaves the open end of the channel acting as a particle reservoir. For the simulation of the unconfined system a cubic simulation box with an extension of 20σ and periodic boundary conditions in x-, y- and z-direction is used containing 3200 particles corresponding to a density of $\rho = 0.4\sigma^{-3}$.

4.1. Density Profile

To analyze the structure of systems in more detail the density profile has been calculated. Fig. 8 shows the density profile perpendicular to the confining walls in y- and z-direction as well as simulation snapshots of the equilibrium configuration. One characteristic property of the density profile is the increased peak at the channel wall which results from the fact, that it is energetically favorable to distribute the particles in such a way that particles with less nearest neighbors close to the wall have smaller separations than those with more neighbors in the center of the channel. This is also the reason why the distance of the first plane is smaller than the distance of adjacent planes in the center of

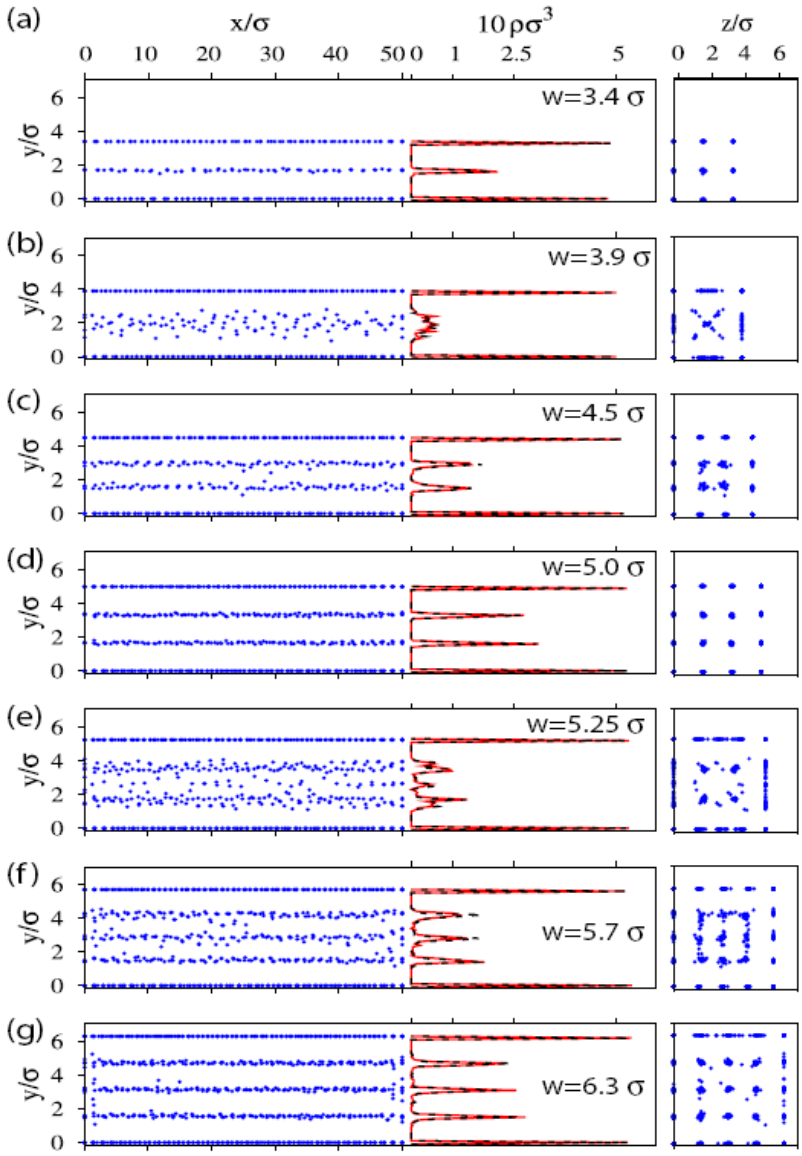

Figure 8. Projection of simulation snapshots of the equilibrium configuration of YHC system ($\kappa\sigma = 1.015$, $U = 432.45$) in 3D microchannels on the xy-plane for different channel widths (left) and average density profile (right) in y-direction (red) and z-direction (black). After Schwierz et al. [44].

the channel. The origin of the oscillations in the structural properties is apparent from the configuration snapshots (Fig. 8): For channel widths smaller than 2σ two planes form - one at each wall. With increasing square section w the particles start to occupy the center of the channel forming a stable mid-plane at $w \approx 3.4\sigma$. This plane forces the wall particles to remain close to the wall thus leading to a minimum in the MSD. If the channel width is further increased the interaction between particles in adjacent planes decreases leading to an increase of the MSD until the mid-plane splits up into two planes and the MSD shows a second minimum at $w = 4.5\sigma$. Until a channel with

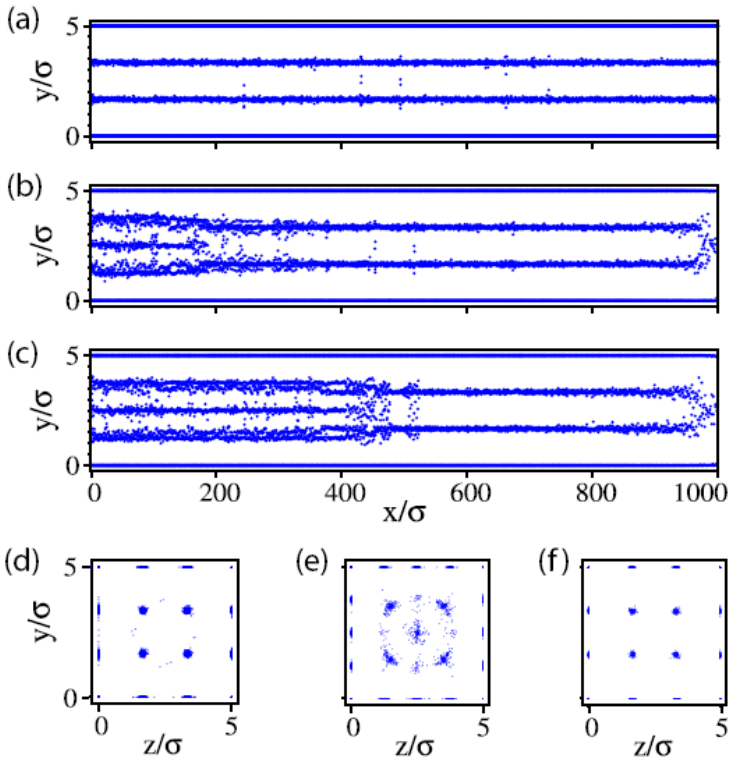

Figure 9. Simulation snapshots of the configuration in a 3D microchannel (a) in equilibrium without an external force, (b) after 10^5 time steps with an external driving force and (c) in the stationary non-equilibrium after 10^6 simulation steps with a constant position of the plane reduction zone within the channel. Projection of simulation snapshots on the yz plane (d) for the equilibrium configuration, (e) for the configuration in the stationary nonequilibrium in the region before the reduction zone, and (f) after the reduction zone. For clarity all particle positions are projected on the xy-plane and the distances in y-direction are stretched by the factor 16. After Schwierz et al. [44].

of $w = 5$ the distance between the planes increases while the particle separation in x-direction decreases. Therefore, the lattice is stretched perpendicular to the confining walls and the MSD shows a minimum. Above $w = 5.25\sigma$ the particle separations in x-direction are so small that it is energetically favorable to form an additional plane. This process continues up to a channel width of $\sim 11\sigma$ whereas maxima in the MSD occur if the distance between adjacent planes is maximal, i.e. if the lattice is stretched normal to the confinement and the interaction between the particles in adjacent planes is minimal. Minima of the MSD occur if an ideal, undistorted lattice can form.

4.2. Transport Behavior of Colloids in 3D Microchannels

Now we address the transport behavior of colloids confined in a 3D microchannel. The colloids are driven by the application of an external driving force. First, we focus on the effect of a reduction of the number of planes i.e. the dynamical rearrangement of the

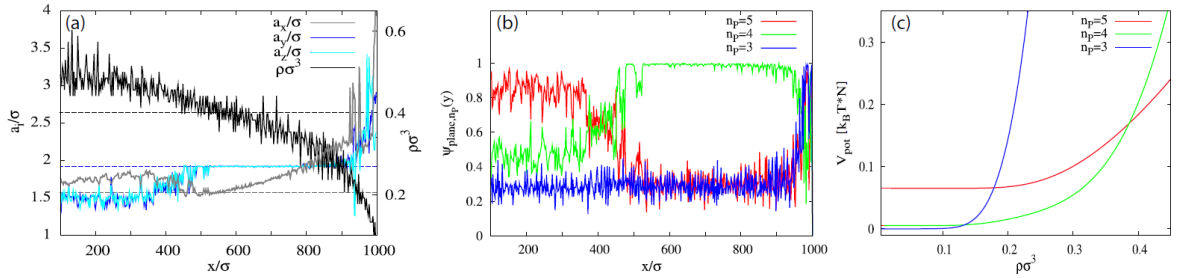

Figure 10. (a) Local density distribution within the channel and lattice constants a_x, a_y and a_z in the stationary non-equilibrium after 10^6 time steps. The dashed lines show the equilibrium values of the local density and the lattice constants. (b) Plane order parameter of the configuration shown in Fig. 9(c). (c) Potential energy for a fcc-lattice in a channel of width 5σ in dependence of the local density for the number of planes in the stationary non-equilibrium. After Schwierz et al. [44].

colloids during their flow along the channel. This phenomenon is analogous to the layer reduction observed in the 2D microchannels [39, 40]. Fig. 9(a) shows the equilibrium configuration in a 3D channel with a quadratic square section of width $w = 5\sigma$ and a length of 1000σ. In equilibrium a loose structure with four planes forms which is stretched perpendicular to the confinement and in which the particles can move away from the wall easily (see Fig. 8(d)). In the stationary non-equilibrium the average drift velocity is $1.43 * 10^{-7}$ m/s which is significantly larger than the drift velocity of non-interacting particles indicating non-plug-flow. Fig. 9 shows the time evolution of the system: In equilibrium a plane structure forms with four planes parallel to the confining walls in y- and z-direction. The external force leads after 10^5 time steps to an additional fifth plane in the reservoir. The area with five planes moves with increasing time in flow direction. Close to the end of the channel the number of planes reduces from four to three planes. After 10^6 time steps the system reaches a stationary non-equilibrium. After that time the position, at which a reduction of the number of planes occurs, does not move in flow direction any more. The transition point oscillates back and forward within a small area. The particles move in planes and layers adapting to the external force. At the transition point the particles have to switch from the mid-plane to one of the adjacent planes closer to the channel wall. Often, particles leave the mid-plane, proceed in flow direction before changing on a plane further outside. The local particle densities and the lattice constants are shown in Fig. 10a and the number of planes is shown in terms of the plane order parameter[44] in Fig. 10b. In the stationary non-equilibrium a density gradient forms along the complete length of the channel causing the change of the number of planes and therefore leading to a change of the lattice constants. At the left end of the channel the lattice constant a_x is larger then a_y and a_z and the lattice is compressed perpendicular to the confinement. In the transition area a_y and a_z increase in two steps in contrast to the 2D systems where the lattice constant a_y shows a single jump. At the end of the transition area a_x is smaller than a_y and a_z. While the latter two remain constant until the next transition point, a_x increases

monotonically. This behavior suggests, that stretching of the lattice in flow direction leads to an instability causing the reduction of the number of planes. The change in the number of planes is clearly visible from the plane order parameter shown in Fig. 10b. The order parameter does not have a sharp transition point but rather a transition area with an extension of about 100σ in which the value changes step like. The reason is that the order parameter of the wall particles drops to zero about 100σ later than the order parameter of the planes in the middle of the channel. Thus, the planes closest to the wall are more stable against a deformation of the lattice. Again, the reduction of the number of planes can be explained by calculating the potential energy per particle in dependence of the local density. Starting from an ideal fcc-crystal with a constant number of planes, i.e. constant distances between the particles in y- and z-direction, the distances in x-direction are increased or decreased and the potential energy is calculated. The dependence of the potential energy on the local density for a constant number of planes is shown in Fig. 10c. Above a value of the local density of $\rho\sigma^3 = 0.38$ it is energetically favorable for the system to form five planes, for values $0.38 > \rho\sigma^3 > 0.13$ four planes and below $\rho\sigma^3 = 0.13$ three planes. These values are slightly smaller than the values at which a reduction occurs in the simulations. This can be explained by the fact that the density in the middle of the channel is smaller than close to the walls (see Fig. 8).

4.3. Diffusion of Model Colloids in 2D Microchannels

In addition, we have studied the effect of the layering in two-dimensional colloidal system on the diffusion behavior. At a constant dimensionless interaction strength and constant density, layered systems and more disordered systems alternate with increasing channel width L_Y, as figure 11 shows. This type of layering order can also be characterized

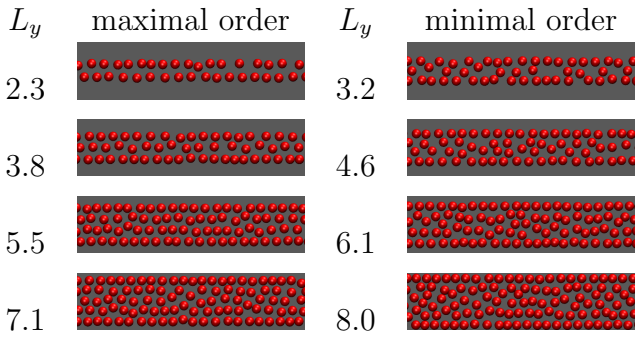

Figure 11. Snapshots of different channel configurations with maximal order (left) and minimal order (right). The diffusion in ordered systems is suppressed whereas the diffusion in disordered systems is enhanced. [46]

by a layer order parameter Ψ_{layer,n_l} [39, 40, 44], which is near 1 if the particles are structured in n_l equidistant layers and otherwise much smaller (Fig. 12 **(a)**). This layering has an important influence on the diffusion, which can be characterized by

the mean square displacement (MSD). Starting from the well known case of single file diffusion [47] at channel width $L_Y = 1$ (Fig. 12 **(b)**) with a long time evolution of the MSD $\langle(\Delta x(t))^2\rangle \propto t^{0.5}$, we studied the dependency of the MSD on the width of the channels. The MSD for wider channels has a non-monotonic dependency on the width L_Y. This non-monotonic behavior is induced by the layering. Fig. 12 **(c)** shows the MSD for the channels with maximal order ($L_Y = 2.3; 3.8; 5.5$) and with minimal order ($L_Y = 3.2; 4.6; 6.1$). The diffusion has a maximum for disordered channels and a minimum for channels with layering. This work is still in progress [46].

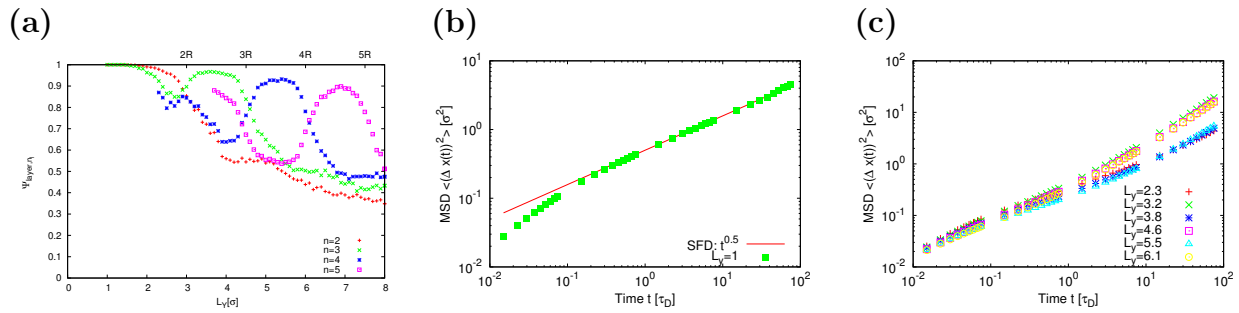

Figure 12. **(a)** The layer order parameters Ψ_{layer,n_l} as a function of channel width for $n_l = 2, 3, 4, 5$ layers. **(b)** and **(c)** show the mean square displacements as function of time in a log-log plot for different channel widths [46].

5. Dynamics of a Two-Dimensional Colloidal Liquid With Pinning

A special way to confine particles is a set of pinning sites distributed randomly within a two-dimensional plane. This $(2D - \epsilon)$-dimensional system is less artificial as it may appear. The thermodynamics of two-dimensional crystallization in random potentials is of particular interest since Nelson discovered the possibility of a melting transition due to quenched random impurities [48]. Chudnovsky and Serota generalized this scenario to substrates with random force fields [49, 50], and Cha and Fertig found a disorder induced melting at zero temperature [51]. In this context, we want to study the effect of confinement due to random pinning on the dynamics of a two-dimensional colloidal system.

Our ensemble consists of epoxy coated, superparamagnetic polystyrene beads with a size of 4.5 μm. Diluted in water and confined in a cylindrical glass cell with a radius of 5 mm and a height of 1.5 mm, the particles sediment down to the bottom glass plate due to their higher mass density. We obtain one monolayer consisting of $\sim 10^5$ particles of which approximately 1 % are pinned to the glass substrate. The pinning occurs due to a linking of epoxy polymers to the glass surface. The system is fixed at room temperature and inclined by precise micrometer motors to ensure a perfect horizontal alignment of the layer. The beads are doped with nanometer sized Fe_2O_3/Fe_3O_4 domains which cause superparamagnetic behavior with a high magnetic susceptibility χ per bead. An external magnetic field H perpendicular to the monolayer aligns the dipoles with particle

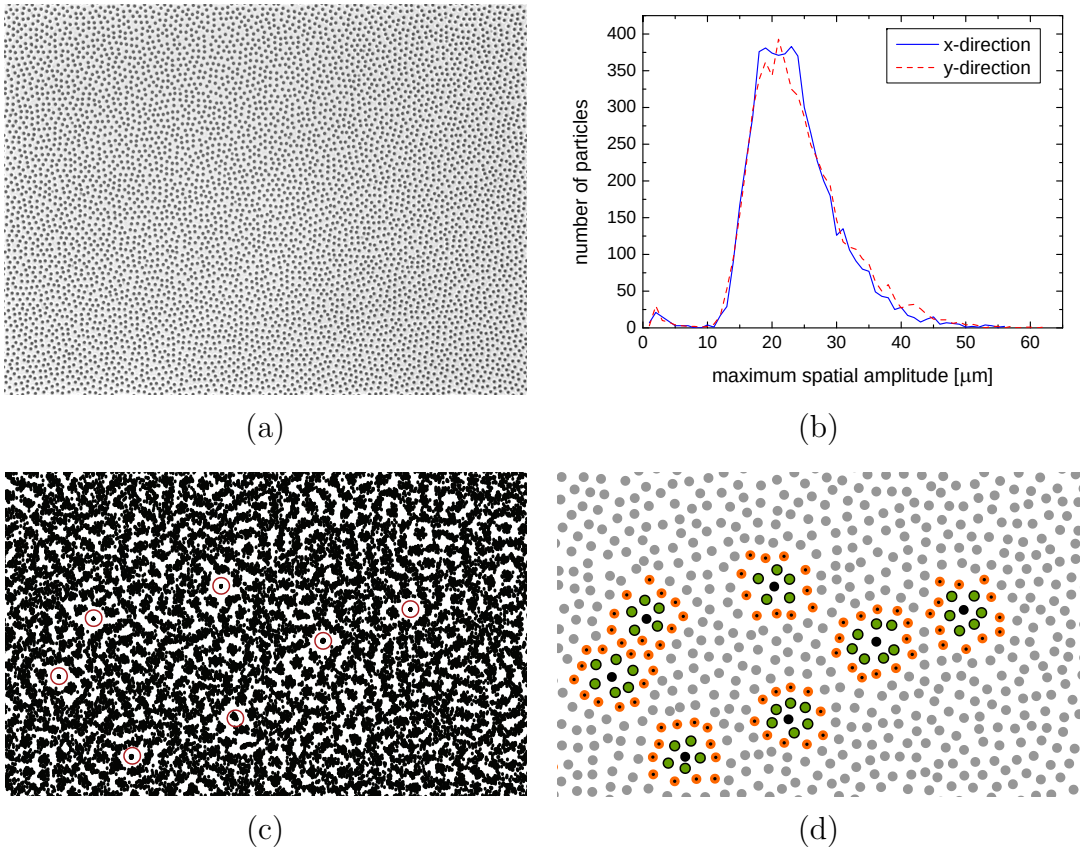

Figure 13. (a): Snapshot of the colloidal ensemble at the first time step. (b): Distribution of the maximum spatial amplitude of the single particle positions during 5000 s. Particles are defined as pinned if their amplitude is below 9 μm. (c): Trajectories after 5000 s in a sub-window of the ensemble. The pinned particles are highlighted with circles. (d): Same sub-window as in (c), division of the ensemble in subsystems: pinned sites (black), their nearest (green) and next nearest neighbors (orange), and the rest of the particles (grey).

density n and allows us to tune the interaction strength between the beads, indicated by the dimensionless parameter

$$\Gamma = \frac{(\pi n)^{3/2} \chi^2 H^2}{4\pi k_B T}. \tag{3}$$

Γ is the ratio of magnetic versus thermal energy which is a measure of the inverse system temperature $1/T$. A window of 1 mm^2 consisting of a few thousand beads is monitored permanently by video microscopy and the particles are tracked for a few hours in steps of a few seconds. This allows us to generate precise static and dynamic correlation functions in the long time limit.

We prepared the colloidal system at an interaction strength of $\Gamma \approx 37.0$. At this value, the system is in the isotropic liquid phase [52]. Figure 1(a) shows a snapshot of our ensemble which consists of approximately 5800 particles. Figure 1(b) shows the distribution of the maximum spatial amplitude of the particles in x- and y-direction. The amplitude is calculated by the magnitude of the difference between the minimum

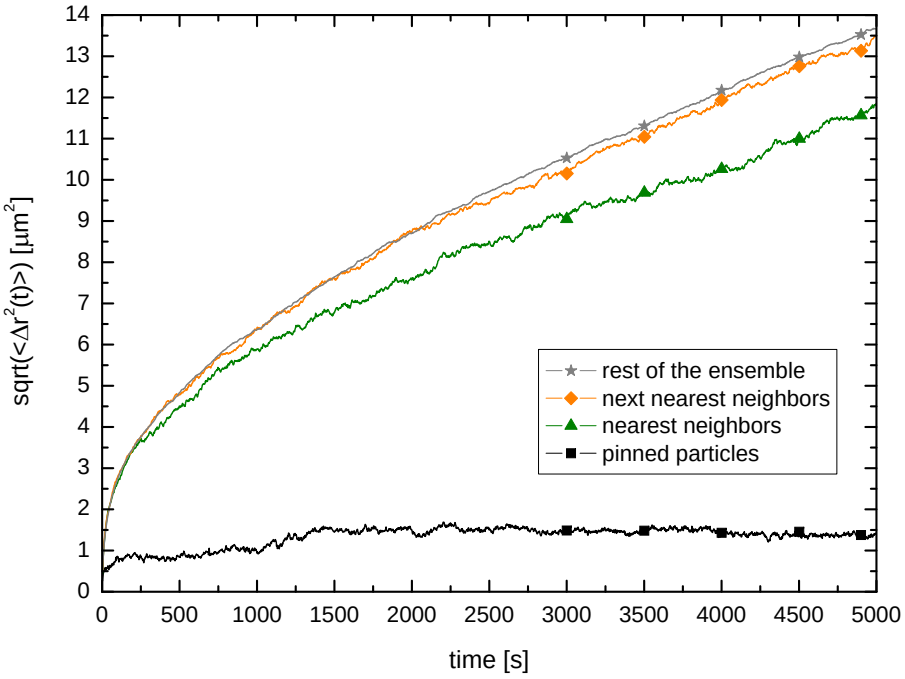

Figure 14. Sqrt-MSD for the different subsystems. The nearest neighbors of the pinned particles show a significant difference in the dynamic in respect to the rest of the ensemble, which is even seen for the next nearest neighbors.

and maximum particle position during 5000 s. One can see, that most particles cover the region with amplitudes between 15 and 35 μm, separated from particles with smaller amplitudes. We define particles as pinned, if their maximum spatial amplitude is less than 9 μm, in x- *and* in y-direction. This threshold is also geometrically reasonable because it is twice the particle diameter and exactly the displacement a particle needs to get out of the way of another one. Figure 1(c) shows a trajectory plot of a sub-window of the colloidal system for 5000 s. The pinned particles are highlighted with circles and one can see, that these particles are clearly restricted in their movement.

We are now interested in the effect of the pinned particles on the dynamics of the rest of the ensemble. This effect should be more crucial for particles near the pinned ones than for the bulk. Therefore we subdivide the system into nearest neighbors and next nearest neighbors of the pinned particles, and the rest of the system. This classification can be seen in Figure 1(d), where the pinned particles are colored black, nearest neighbors green, next nearest neighbors orange and the rest of the ensemble grey. To study the dynamics of the different subsystems, we look at the characteristics of the mean square displacement

$$\left\langle \Delta\vec{r}^{\,2}(t) \right\rangle = \frac{1}{N}\sum_{i=1}^{N} |\vec{r}_i(t) - \vec{r}_i(0)|^2 \tag{4}$$

where the sum runs over all particles N. The result is shown in Figure 2 for the different subsystems, where the square root of the mean square displacement (sqrt-

MSD) is plotted. One can see, that there is a significant difference in the dynamic for the nearest neighbors observable, compared to freely moving particles in the bulk. This is caused by their partial confinement due to the pinned particles. There is even a slight drop in the sqrt-MSD for the next nearest neighbors in the second shell, what indicates that the restricted dynamic due to the confinement is transferred over 'free' particles. For the pinned particles the sqrt-MSD is bounded at long times. It is interesting to note that the timescale, where deviations between first shell and bulk particles are visible ($\sim$ 250 s), is comparable to a few Brownian timescales.

The dynamic of the nearest neighbors is clearly constricted and this effect is even seen for the next nearest neighbors. Approaching a more ordered phase, this might have a crucial effect on transition temperatures, the character and the microscopic mechanism of the phase transition. Not only, that fluctuations on all length scales might be suppressed which are essential for the KTHNY melting scenario [53, 54, 55], a system with random pinning might also show similar thermodynamics as systems with short or long scale disordered substrates [56] or in confined geometries [17].

6. Concluding Remarks

In this paper, we have presented model calculations on colloidal systems in either strictly two-dimensional geometry, considering also the effect of confinement to quasi-one-dimensional slit pores or channnels, and dealing also with transport in quasi-one-dimensional channels having a square cross section. One of the perturbations of the ordering that we considered was the uniaxial compression of colloidal crystals (that in the ideal case form a perfect triangular lattice structure) by corrugated walls, that (in the case without misfit) are commensurate with the crystal structure. We have studied the phase transitions that occur in the number of layers that take place with increasing misfit (n layers $\rightarrow n-1$ layers $\rightarrow n-2$ layers). We studied the increasing disorder, that this compression (together with the resulting incommensurability at the walls) causes. Since these transitions display huge hysteresis, and also in some cases several different structures occur with comparable degree of disorder, it has not been clear which of these structures is the stable one, and which are only metastable. For answering such questions, we found it useful to develop methods from which the free energy differences between different (partially ordered) structures can be inferred. Comparing results obtained from either the Schmid -Schilling method or the "phase switch Monte Carlo"-method of Wilding, we found that both methods give mutually compatible results, but the phase switch Monte Carlo method gives much more accurate results even with less numerical effort. We believe that this method should also be useful for other cases where in colloidal systems several (partially or perfectly) ordered phases compete with each other. Another interesting perturbation occurs if the two confining walls are not used to compress the system in the direction perpendicular to the walls,but rather to create a shear deformation,moving both walls along the strip,but in antiparallel directions. This causes a kind of "melting" of a few layers of the crystal along the wall.The behavior

of such a deformed crystal is reminiscent of "shear banding", familiar from other soft matter systems under flow; however, the investigation of the details of this interesting behavior must be left to future work.

In conclusion, our studies on binary hard-disk mixtures using Monte Carlo simulations [3] showed, that complex lattice structures in binary hard-disk mixtures form thermodynamically stable phases only in a high pressure environment. An alternative, successful route to the controlled structuring of such binary mixtures is exposing the system to a modulated external field. Weak external fields allow a controlled tuning of the miscibility of the mixture. The ordering mechanisms resulting in a laser induced demixing (LID) in this regime depends on the details of the coupling of the components of the mixture to the modulating field [3, 4].

In addition, a structural analysis has been performed in colloidal model system with dipolar of YHC particle interactions in 2D and 3D microchannels. We have reported on a variety of ordering and transport phenomena induced by the confinement of the motion of the particles by parallel walls and by the application of a constant driving force along the channel. The structural properties show oscillations upon increasing the width of the channel with a period of the effective boundary plane distance. When the channel width is increased, a periodic destabilization of the plane structure with n_p planes takes place, and the system switches to a structure with $n_p + 1$ planes. Moreover, we have shown that the number of planes can be reduced by applying an external driving force. In the stationary nonequilibrium the particles flow over the reduction zone which stays at a constant position. For small driving forces, where the particles are not in the regime of plug flow, the particles arrange themselves into a different number of planes analogous to the rearrangement into layers in the 2D systems. The reduction originates from a density gradient along the channel, and the phenomenon of layer reduction appears to be independent of the exact form of the interaction potential and occurs likewise in 2D and 3D systems if the range of the interaction potential is larger than the average distance between neighboring particles. The effect of the layering in 2D systems on the diffusion behavior is briefly discussed.

In an experimental system we have shown that point like defects can affect the mobility of particles locally. The mean squared displacement of particles being nearest neighbors of particles which are immobile due to pinning to the substrate is significantly reduced in a 2D fluid. The effect is even visible in the second shell of pinned particles. This locally reduced mobility caused by pinning centers may affect the nature of phase transition in 2D experimental systems where critical fluctuations play an important role.

Acknowledgments

The authors thank the SFB-TR6 for support and the NIC for computer time. Some of us (D.W., K.B., P.V.) also thank Surajit Sengupta and Nigel B.Wilding for their valuable collaboration on simulations of colloidal crystals confined by corrugated walls, and they also thank T. Schilling, F. Schmid, and I. Snook for helpful discussions.

References

[1] Franzrahe K, Nielaba P, Sengupta S 2010 *Phys. Rev. E* **82** 016112
[2] Franzrahe K, Keim P, Maret G, Nielaba P, Sengupta S 2008 *Phys.Rev. E* **78** 026106
[3] Franzrahe K, Nielaba P 2009 *Phys. Rev. E* **79** 051505
[4] Franzrahe K and Nielaba P 2007 *Phys. Rev. E* **76** 061503
[5] Bürzle F, Nielaba P 2007 *Phys. Rev. E* **76** 051112
[6] Strepp W, Sengupta S and Nielaba P 2001 *Phys. Rev. E***63** 046106
[7] Strepp W, Sengupta S and Nielaba P 2002 *Phys. Rev. E***66** 056109
[8] Lue L and Woodcock LV 1999 *Mol. Phys.* **96** 1435
[9] Likos CN, Henley CL 1993 *Phil. Mag. B* **68** 85
[10] Chowdhury A and Ackerson BJ 1985 *Phys. Rev. Lett.* **55** 833
[11] Wei QH, Bechinger C, Rudhardt D and Leiderer P 1998 *Phys. Rev. Lett.* **81** 2606
[12] Chakrabarti J, Krishnamurthy HR, Sood AK and Sengupta S 1995 *Phys. Rev. Lett.* **75** 2232
[13] Chaudhuri P, Das C, Dasgupta C, Krishnamurthy HR and Sood AK 2005 *Phys. Rev. E* **72** 061404
[14] Chakrabarti J, Krishnamurthy HR and Sood AK 1994 *Phys. Rev. Lett.* **73** 2923
[15] Frey E, Nelson DR and Radzihovsky L 1999 *Phys. Rev. Lett.* **83** 2977
[16] Radzihovsky L, Frey E and Nelson DR 2001 *Phys. Rev. E* **63** 031503
[17] Ricci A, Nielaba P, Sengupta S, and Binder K 2006 *Phys. Rev. E* **74** 010404(R)
[18] Ricci A, Nielaba P, Sengupta S, and Binder K 2007 *Phys. Rev. E* **75** 011405
[19] Chui Y-H, Sengupta S, and Binder K 2008 *EPL* **83** 58004
[20] Chui Y-H, Sengupta S, Snook IK, and Binder K 2010 *J. Chem. Phys.* **132** 074701
[21] Chui Y-H, Sengupta S, Snook IK, and Binder K 2010 *Phys. Rev. E* **81** 020403(R)
[22] Schilling T and Schmid F 2009 *J. Chem. Phys.* **131** 231102
[23] Wilms D, Wilding NB and Binder K 2012, preprint
[24] Bruce AD, Wilding NB and Ackland GJ 1997 *Phys. Rev. Lett.* **79** 3002
[25] Wilding NB and Bruce AD 2000 *Phys. Rev. Lett.* **85** 5138
[26] Wilms D, Virnau P, Sengupta S and Binder K 2012, preprint
[27] Löwen H 2001 *J. Phys.: Condensed Matter* **13** R415
[28] Roth R and Gillespie D 2005 *Phys. Rev. Lett.* **95** 247801
[29] Squires TM and Quake SR 2005 *Rev. Mod. Phys.* **77** 977
[30] Helbing D, Molnar P, Farkas I and Bolay K 2001 *Environ. Plann. B Plann. Des.* **28** 361
[31] Rex M, Löwen H and Likos CN 2005 *Phys. Rev. E* **72** 021404
[32] Rex M and Löwen H 2007 *Phys. Rev. E* **75** 051402
[33] Rex M and Löwen H 2008 *Eur. Phys. J. E* **26** 143
[34] Chakrabarti J, Dzubiella J and Löwen H 2004 *Phys. Rev. E***70** 012401
[35] Dzubiella J and Löwen H 2002 *J. Phys.: Condens. Matter* **14**
[36] Chakrabarti J, Dzubiella J and Löwen H 2003 *EPL* **61** 415
[37] Leunissen ME, Christova CG, Hynninen AP, Royall CP, Campbell AI, Imhof A, Dijkstra M, v. Roij R and v. Blaaderen A 2005 *Nature* **437** 235
[38] Sütterlin KR, Wysocki A, Ivlev AV, Räth C, Thomas HM, Rubin-Zuzic M, Goedheer WJ, Fortov VE, Lipaev AM, Molotkov VI, Petrov OF, Morfill GE and H. Löwen H 2009 *Phys. Rev. Lett.* **102** 085003
[39] Köppl M, Henseler P, Erbe A, Nielaba P and Leiderer P 2006 *Phys. Rev. Lett.* **97** 208302
[40] Henseler P, Erbe A, Köppl M, Leiderer P and Nielaba P 2010 *Phys. Rev. E* **81** 041402
[41] Schmittmann B and Zia RKP 1995 *Phase Transition and Critical Phenomena* **17**, ed. (Academic,1995).
[42] Haghgooie R and Doyle PS 2004 *Phys. Rev. E* **70** 061408
[43] Piacente G and Peeters FM 2005 *Phys. Rev. B* **72** 205208
[44] Schwierz N and P. Nielaba P 2010 *Phys. Rev. E* **82** 031401
[45] Ermak DL 1975 *J. Chem. Phys.* **62** 4189

[46] Siems U, Dissertation (U. Konstanz) in preparation
[47] Wei QH, Bechinger C and Leiderer P 2000 *Science* **287** 625
[48] Nelson DR 1983 *Phys. Rev. B* **27**(5) 2902
[49] Chudnovsky EM 1986 *Phys. Rev. B* **33**(1) 245
[50] Serota RA 1986 *Phys. Rev. B* **33**(1) 3403
[51] Cha M-C and Fertig HA 1995 *Phys. Rev. Lett.* **74**(24) 4867
[52] Keim P, Maret G and von Grünberg HH 2007 *Phys. Rev. E* **75** 031402
[53] Kosterlitz JM and Thouless DJ 1973 *J. Phys. C* **6** 1181
[54] Halperin BI and Nelson DR 1978 *Phys. Rev. Lett.* **41**(7) 519
[55] Young AP 1979 *Phys. Rev. B.* **19**(4) 1855
[56] Carpentier D and Le Doussal P 1998 *Phys. Rev. Lett.* **81**(9) 1881